Nonlinear Dyn (2012) 70:421–434
DOI 10.1007/s11071-012-0465-4

ORIGINAL PAPER

A novel scheme for nonlinear displacement-dependent dampers

Shahab Ilbeigi · Javad Jahanpour · Anooshiravan Farshidianfar

Received: 21 February 2012 / Accepted: 17 May 2012 / Published online: 7 June 2012

Abstract In this paper, a novel scheme for nonlinear displacement-dependent (NDD) damper is introduced. The damper is attached to a simple mass-spring-damper vibration system. The vibration system equipped with a NDD damper is mathematically modeled and the nonlinear governing differential equation of the system is derived. To obtain the displacement of the system, the approximate analytical solution of the governing equation is elaborated using the multiple scales method. The advised approximate analytical algorithm is performed for several case studies and is also verified by the numerical fourth-order Runge–Kutta method. In addition, the performance of the NDD damper is analyzed and compared with the performance of the traditional linear damper. It is found that the proposed NDD damper scheme along with the multiple scales method is not only feasible for vibration reduction but also yields satisfactory response performance rather than the existing traditional linear damper.

Keywords Displacement-dependent damper · Nonlinear differential equation · Vibration reduction · Perturbation · Multiple scales method

S. Ilbeigi
Department of Mechanical Engineering, Bu-Ali Sina University of Hamedan, Hamedan, Iran

J. Jahanpour (✉)
Department of Mechanical Engineering, Mashhad Branch, Islamic Azad University, Mashhad, Iran
e-mail: jahanpourfr@mshdiau.ac.ir

A. Farshidianfar
Department of Mechanical Engineering, Ferdowsi University of Mashhad, Mashhad, Iran

1 Introduction

In many applications, vibration may cause discomfort, disturbance, damage, and sometimes destruction of the system or the structure. A general method for reducing these effects is adding a viscous damper to the vibration system. Many of viscous dampers have a constant damping coefficient; however, variable dampers have already found their way to commercial applications [1, 2].

In point of view of controllability, variable dampers can be classified as passive, active, and semiactive [3–7]. Passive dampers have fixed properties which are determined and preset according to the design goals and intended application [8]. Active dampers are operated by using an external power which in most cases is provided by hydraulic actuators [9–11]. The main disadvantages of active dampers are their high power consumption, size, heavy weight, and cost. Semiactive dampers are a compromise between the active and passive dampers [12].

Despite the higher performance of active and semiactive dampers, passive dampers are still the most

widely used ones [2]. Although there are many types of passive dampers, the passive variable damper has been recently developed. Among the passive variable dampers, those with stroke and displacement/position sensitivity have been studied in several works. Venkatesan and Krishnan [13] presented the application of dual-phase damping to a simple shock mount wherein the damping coefficient was a function of relative displacement between the foundation and the mounted mass. Haque et al. [14] carried out an analysis of displacement sensitive dual-phase dampers by transforming the displacement sensitive coefficient into a velocity sensitive coefficient. Hundal [15] analyzed an impact absorber consisting of a linear spring in parallel with a hydraulic damper with two-stage variable area orifice. Fukushima et al. [16] suggested that dampers should have a stroke dependent characteristic, such that for a given velocity a longer stroke would give a greater force. However, the force in the stroke sensitivity cannot be identified directly with the actual position of the piston in the cylinder [1]. The effect of the rubber mounting bushes in introducing some stroke sensitivity to the vibration systems has been investigated in [17–19]. Lee and Moon [20, 21] reported on tests of a displacement sensitive damper with a longitudinally grooved pressure cylinder to relax the damping around the central position. In this method, machining the grooves would require a thicker basic cylinder wall than would otherwise be used, as this is usually only about one millimeter [1]. Application of displacement sensitive dampers has also some history on aircraft landing gear, motorcycles, and cars. The displacement sensitive schemes for landing gears utilize positive recoil control or two and three level position dependent damping [22]. In a motorcycle front fork, a short and blunt rubber as a needle causes the damper orifice to get closed which allows weaker springing with improved ride quality pressure [1]. The displacement sensitive damper suggested for vehicle suspension application follows the idea of using a long tapered needle entering an orifice in the piston [1, 23]. This type of damper is merely limited to employing a tapered needle and is not mathematically modeled.

Some researchers have recently investigated thoroughly the nonlinear dampers [7, 24, 25]. For instance, Farjoud et al. [24] presented a nonlinear model of monotube hydraulic dampers with an emphasis on the effects of shim stack on damper performance. Also, Guo et al. [25] studied the force and displacement transmissibility of nonlinear viscous damper based vibration isolation.

In this paper, a novel scheme for Nonlinear Displacement-Dependent (NDD) damper is proposed. The novelty of this work is that the proposed NDD damper scheme takes the advantage of the special geometric shape rather than the tapered needle. The geometric shape is defined by introducing two parameters which includes a large variety of shapes. In contrast with the discussed dampers in the literature review, in the proposed NDD damper, the damping coefficient and the damping force are continuous and smooth functions of displacement. Furthermore, in this paper, the nonlinear governing differential equation of a mass-spring-damper system equipped with the NDD damper is derived. To obtain the displacement of the system, the approximate analytical solution of the governing equation is elaborated using the multiple scales method (MSM).

The rest of the paper is organized as follows. Section 2 describes the mechanism of the proposed NDD damper. In Sect. 3, the mathematical model of the NDD damper in a mass-spring-damper system is formulated. The approximate analytical solution of the system is obtained in Sect. 4. Some numerical examples are presented in Sect. 5, and the results are analyzed and discussed in Sect. 6. Finally, Sect. 7 concludes the paper.

2 The NDD damper mechanism

A simple viscous damper consists of a moving piston having one or some orifices inside a cylinder filled with a viscous fluid (Fig. 1). Velocity of the piston and the damping force are related linearly as follows:

$$F = c\frac{\mathrm{d}u}{\mathrm{d}t} \tag{1}$$

where c is the damping coefficient.

Assuming the piston has one orifice, by taking advantage of the Hagen–Poiseuille equation for the laminar flow, c can be obtained by

$$c = \lambda\left[\left(\frac{D}{d}\right)^2 - 1\right]^2 \tag{2}$$

where D and d are the cylinder diameter and the opening fluid gap diameter, respectively. Also, $\lambda = 8\pi\mu L$

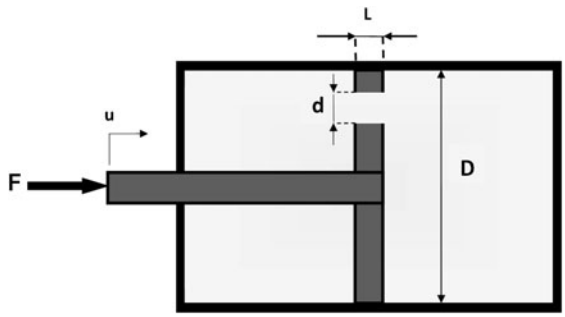

Fig. 1 Schematic of a simple viscous damper

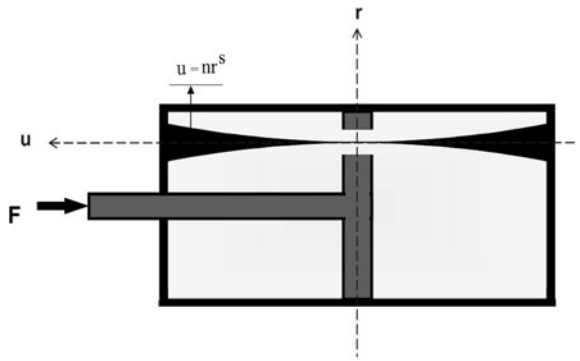

Fig. 2 Schematic of the designed nonlinear displacement-dependent damper

in which, μ denotes for dynamic viscosity of the fluid and L is the piston width.

For a set of selected parameters D, d, and L, the damping coefficient has a constant value. The mechanism can be designed to make the linear damper into nonlinear and displacement-dependent. To this end, a function in Cartesian r–u coordinates is considered as

$$u = nr^s \tag{3a}$$

or

$$r = \left(\frac{u}{n}\right)^{\frac{1}{s}}. \tag{3b}$$

A solid cone shaped part can be generated by rotating the interior region of the aforementioned function around the u-axis. Now the cone shaped part must get assembled into the linear damper, so that the origin of coordinates is located on the center of the piston opening. The cone shaped part must be fixed to make the fluid travel through its outer surface and the inner surface of the orifice (Fig. 2). According to Fig. 2, during the motion of the piston, the opening fluid gap is changed and the damping coefficient is consequently varied. Therefore, the ordinary linear damper with a constant damping coefficient is converted to the nonlinear damper with a variable displacement-dependent damping coefficient.

3 Mathematical formulation of the NDD damper

For the designed displacement-dependent damping mechanism shown in Fig. 2, the opening fluid gap diameter is equal to $d - 2r$.

Therefore, it is needed to substitute $d - 2r$ for d into Eq. (2) as follows:

$$c = \lambda\left[\left(\frac{D}{d-2r}\right)^2 - 1\right]^2. \tag{4}$$

Substituting for r from Eq. (3b) leads to

$$c = \lambda\left[\gamma^2\left(\frac{1}{1-\beta u^{(\frac{1}{s})}}\right)^2 - 1\right]^2 \tag{5}$$

where $\beta = \frac{2}{d \cdot n^{(\frac{1}{s})}}$ and $\gamma = \frac{D}{d}$.

Due to the fact that the damper stroke is small, Eq. (5) can be expanded and simplified by the following Taylor series expansion:

$$\frac{1}{1-\beta u^{(\frac{1}{s})}} = 1 + \beta u^{(\frac{1}{s})} + O\left(u^2\right). \tag{6}$$

Thus, Eq. (5) can be expressed as

$$c = \alpha_1 + \alpha_2 |u|^{(\frac{1}{s})} + \alpha_3 |u|^{(\frac{2}{s})} + \alpha_4 |u|^{(\frac{3}{s})} + \alpha_5 |u|^{(\frac{4}{s})}. \tag{7}$$

For the case of $n = 1$ and $s = \frac{1}{2}$, Eq. (7) will be rewritten as follows:

$$c = \alpha_1 + \alpha_2 u^2 + \alpha_3 u^4 + \alpha_4 u^6 + \alpha_5 u^8. \tag{8}$$

The parameters α_i in Eq. (8) are given in Appendix A.

The governing differential equation of a simple mass–spring–damper system without any external force is as follows:

$$\ddot{u} + \frac{c}{m}\dot{u} + \omega^2 u = 0. \tag{9}$$

For a linear damper with constant damping coefficient, the free oscillation response of the system is as follows [26]:

$$u(t) = \mathrm{e}^{-\zeta\omega t}\Big[u_0\cos\big(\sqrt{1-\zeta^2}\omega t\big) + \frac{\dot{u}_0+\zeta\omega u_0}{\sqrt{1-\zeta^2}\omega}\sin\big(\sqrt{1-\zeta^2}\omega t\big)\Big] \tag{10}$$

where $u_0, \dot{u}_0$, and ζ are initial displacement, initial velocity, and damping ratio, respectively. Besides, the damping force and the total force transmitted to the base can be calculated by the following equations:

$$F_{\text{damping}} = c\frac{\mathrm{d}u(t)}{\mathrm{d}t}, \tag{11}$$

$$F_{\text{Transmitted}} = c\dot{u} + ku. \tag{12}$$

In order to achieve the governing differential equation of a basic mass–spring system equipped with NDD damper, c from Eq. (8) must be replaced into dimensionless form of Eq. (9) as follows:

$$\frac{\mathrm{d}^2u}{\mathrm{d}\hat{t}^2} + u = -\varepsilon\big(1+\beta_1u^2+\beta_2u^4+\beta_3u^6+\beta_4u^8\big)\frac{\mathrm{d}u}{\mathrm{d}\hat{t}}. \tag{13}$$

In which $\hat{t} = \omega t$, $\varepsilon = \frac{\lambda(\gamma^4-2\gamma^2+1)}{m\omega}$ and $\beta_i = \frac{\alpha_i}{m\omega\alpha_1}$.

A perturbation technique by adding a small term to the mathematical description (ε in this paper) can be used to find an approximate solution to the governing differential equation (13) for the case of utilizing the designed NDD damper. The parameter ε is directly proportional to λ and, accordingly, to the fluid viscosity. It is also dependent to γ. Hence, increasing the viscosity or increasing γ, causes increasing ε, and strength of nonlinearity in Eq. (13), successively.

The shape parameters, i.e., n and s, effect on β as $\beta = \frac{2}{d\cdot n^{(\frac{1}{s})}}$ and on the damping coefficient c (as given by Eq. (5)). Accordingly, the dimensionless form of the governing equation of the vibration system utilizing the NDD damper is affected by these shape parameters (see Eq. (13)). It should be noted that the values of the shape parameters n and s do not have any effect on ε, which describes the strength of nonlinearity of the governing equation. Since the main focus of this work is to introduce a novel scheme for NDD dampers, the shape parameters have been selected as a fixed set for a general application as a mass–spring–damper vibration system. Nevertheless, the couple of the values of these parameters can be optimized according to the design goal and intended particular application.

In the following section, the procedure of employing multiple scales method as a perturbation technique is illustrated to solve Eq. (13).

4 Multiple scales method

The underlying idea of multiple scales is to consider the response to be a function of multiple independent variables or scales, instead of a time variable [27, 28]. For this aim, new independent variables must be introduced according to

$$T_n = \varepsilon^n\hat{t} \quad \text{for } n = 0, 1 \text{ and } 2. \tag{14}$$

The asymptotic approximate solution of Eq. (13) can be represented in the form

$$u = u_0(T_0,T_1,T_2) + \varepsilon u_1(T_0,T_1,T_2) + \varepsilon^2u_2(T_0,T_1,T_2) + O\big(\varepsilon^3\big). \tag{15}$$

The first and second derivatives with respect to $\hat{t}$ are in the following form:

$$\begin{aligned}\frac{\mathrm{d}}{\mathrm{d}\hat{t}} &= D_0 + \varepsilon D_1 + \varepsilon^2D_2,\\ \frac{\mathrm{d}^2}{\mathrm{d}\hat{t}^2} &= D_0 + 2\varepsilon D_0D_1 + \varepsilon^2\big(D_1^2 + 2D_0D_2\big)\end{aligned} \tag{16}$$

where $D_n = \frac{\partial}{\partial T_n}$.

Substituting Eq. (15) and Eq. (16) into Eq. (13) and equating coefficients of each power of ε to zero, leads to

$$D_0^2u_0 + u_0 = 0, \tag{17}$$

$$\begin{aligned}&D_0^2u_1 + u_1\\ &= -2D_0D_1u_0\big(1+\beta_1u_0^2 + \beta_2u_0^4+\beta_3u_0^6+\beta_4u_0^8\big)D_0u_0.\end{aligned} \tag{18}$$

$$\begin{aligned}&D_0^2u_2 + \omega^2u_2\\ &= -2D_0D_1u_1 - 2D_0D_2u_0 - D_1^2u_0\\ &\quad - \big(1+\beta_1u_0^2+\beta_2u_0^4+\beta_3u_0^6+\beta_4u_0^8\big)D_0u_1\end{aligned}$$

$$-\left(1+\beta_1 u_0^2+\beta_2 u_0^4+\beta_3 u_0^6+\beta_4 u_0^8\right)D_1 u_0$$
$$-\left(2\beta_1 u_0 u_1+4\beta_2 u_0^3 u_1+6\beta_3 u_0^5 u_1\right.$$
$$\left.+8\beta_4 u_0^7 u_1\right)D_0 u. \tag{19}$$

The general solution of Eq. (17) can be expressed as

$$u_0 = A(T_1,T_2)\mathrm{e}^{\mathrm{i}T_0}+\bar{A}(T_1,T_2)\mathrm{e}^{-\mathrm{i}T_0}. \tag{20}$$

Substituting for u_0 from Eq. (20) into Eq. (18) gives

$$D_0^2 u_1+\omega^2 u_1 = -\mathrm{i}\left[\Delta_1\mathrm{e}^{\mathrm{i}T_0}+\Delta_2\mathrm{e}^{3\mathrm{i}T_0}+\Delta_3\mathrm{e}^{5\mathrm{i}T_0}\right.$$
$$\left.+\Delta_4\mathrm{e}^{7\mathrm{i}T_0}+\Delta_5\mathrm{e}^{9\mathrm{i}T_0}+\mathrm{CC}\right] \tag{21}$$

in which, $\Delta_i{}'$s are given in Appendix A and CC stands for complex conjugate.

Omitting the terms that produce secular terms leads to solvability for the first-order approximation, therefore, the coefficients of $\mathrm{e}^{\pm\mathrm{i}T_0}$ should be vanished; that is,

$$\Delta_1 = 0. \tag{22}$$

The solution of Eq. (21) can be written in the form

$$u_1 = B(T_1,T_2)\mathrm{e}^{\mathrm{i}T_0}+\frac{1}{8}\mathrm{i}\Delta_2\mathrm{e}^{3\mathrm{i}T_0}+\frac{1}{24}\mathrm{i}\Delta_3\mathrm{e}^{5\mathrm{i}T_0}$$
$$+\frac{1}{48}\mathrm{i}\Delta_4\mathrm{e}^{7\mathrm{i}T_0}+\frac{1}{80}\mathrm{i}\Delta_5\mathrm{e}^{9\mathrm{i}T_0}+\mathrm{CC}. \tag{23}$$

In order to solve Eq. (22), one let

$$A = \frac{1}{2}a(T_1,T_2)\mathrm{e}^{\mathrm{i}\phi(T_1,T_2)}. \tag{24}$$

Substituting Eq. (24) and its conjugate and derivatives into Eq. (22) leads to

$$-\left(\frac{\partial a}{\partial T_1}+\mathrm{i}a\frac{\partial\phi}{\partial T_1}\right) = \frac{1}{256}\left(128a+32\beta_1 a^3+16\beta_2 a^5\right.$$
$$\left.+10\beta_3 a^7+7\beta_4 a^9\right). \tag{25}$$

Separating real and imaginary parts in Eq. (25) results in

$$\frac{\partial\phi}{\partial T_1} = 0, \tag{26a}$$
$$\frac{\partial a}{\partial T_1} = -\frac{1}{256}\left(128a+32\beta_1 a^3+16\beta_2 a^5\right.$$
$$\left.+10\beta_3 a^7+7\beta_4 a^9\right). \tag{26b}$$

Hence, $\phi=\phi(T_2)$ and $a(T_1,T_2)$ can be solved by integration from Eq. (26b).

To determine the second-order approximation to u, u_0 , and u_1 from Eq. (20) and Eq. (23) must be substituted into Eq. (19) as follows:

$$D_0^2 u_2+u_2 = Q(T_1,T_2)\mathrm{e}^{\mathrm{i}T_0}+\bar{Q}(T_1,T_2)\mathrm{e}^{-\mathrm{i}T_0}$$
$$+\mathrm{NST} \tag{27a}$$

where NST stands for Non-Secular Terms and

$$Q(T_1,T_2) = -\mathrm{i}\left(B+\beta_1 A^2\bar{B}+2\beta_1 A\bar{A}B+4\beta_2 A^3\bar{A}\bar{B}\right.$$
$$+6\beta_2 A^2\bar{A}^2 B+15\beta_3 A^4\bar{A}^2\bar{B}$$
$$+20\beta_4 A^3\bar{A}^3 B+56\beta_4 A^5\bar{A}^3\bar{B}$$
$$\left.+70\beta_4 A^4\bar{A}^4 B\right)-D_1^2 A-2\mathrm{i}D_1 B$$
$$-2\mathrm{i}D_2 A-\left(1+2\beta_1 A\bar{A}+6\beta_2 A^2\bar{A}^2\right.$$
$$+20\beta_3 A^3\bar{A}^3+70\beta_4 A^4\bar{A}^4\left.\right)D_1 A$$
$$-\left(\beta_1 A^2+4\beta_2 A^3\bar{A}+15\beta_3 A^4\bar{A}\right.$$
$$\left.+56\beta_4 A^5\bar{A}^3\right)D_1\bar{A}+q(T_1,T_2) \tag{27b}$$

in which $q(T_1,T_2)$ is given in Appendix A. Secular terms will be eliminated if $Q=0$. To solve Eq. (27b) with $Q=0$, one let

$$B = \frac{1}{2}\mathrm{i}b\mathrm{e}^{\mathrm{i}\phi}. \tag{28}$$

Substituting for A and B from Eqs. (24) and (28) into Eq. (27b) with $Q=0$ and separating real and imaginary parts yields

$$\mathrm{i}\left(\frac{1}{8}\beta_1 a^3\frac{\partial\phi}{\partial T_1}+\frac{1}{2}a\frac{\partial\phi}{\partial T_1}-\frac{1}{8}\beta_1 a^3\frac{\partial\phi}{\partial T_1}+\frac{\partial a}{\partial T_1}\frac{\partial\phi}{\partial T_1}\right.$$
$$+\frac{1}{2}a\frac{\partial^2\phi}{\partial T_1^2}-b\frac{\partial\phi}{\partial T_1}+\frac{\partial a}{\partial T_2}\left.\right)+\left(-\frac{1}{8}\beta_1 a^2 b-\frac{1}{2}b\right.$$
$$+\frac{3}{8}\beta_1 a^2\frac{\partial a}{\partial T_1}+\frac{1}{2}\frac{\partial a}{\partial T_1}+\frac{1}{2}\frac{\partial^2 a}{\partial T_1^2}-\frac{1}{2}a\left(\frac{\partial\phi}{\partial T_1}\right)^2$$
$$\left.-\frac{\partial b}{\partial T_1}-a\frac{\partial\phi}{\partial T_2}-\frac{1}{256}\beta_1^2 a^5\right)=0. \tag{29}$$

Substituting Eq. (26a) in the real and imaginary parts of Eq. (29) gives

$$\frac{\partial a}{\partial T_2}=0 \quad\rightarrow\quad a=a(T_1), \tag{30}$$

$$2\frac{\partial b}{\partial T_1}+\left(1+\frac{1}{4}\beta_1 a^2\right)b = -2a\frac{\mathrm{d}\phi}{\mathrm{d}T_2}+\frac{\mathrm{d}^2 a}{\mathrm{d}T_1^2}+\left(1+\frac{3}{4}\beta_1 a^2\right)\frac{\mathrm{d}a}{\mathrm{d}T_1} - \frac{1}{128}\beta_1^2 a^5. \tag{31}$$

With the help of Eq. (26b), Eq. (31) can be expressed as

$$2\frac{\partial b}{\partial T_1}+2\frac{b}{a}\frac{\mathrm{d}a}{\mathrm{d}T_1} = -2a\left(\frac{\mathrm{d}\phi}{\mathrm{d}T_2}+\frac{1}{16}\right) + \left(\frac{1}{4}+\frac{7}{16}\beta_2 a^2\right)\frac{\mathrm{d}a}{\mathrm{d}T_1}. \tag{32}$$

Thus,

$$\mathrm{d}\left(\frac{b}{a}\right) = -\left(\frac{\mathrm{d}\phi}{\mathrm{d}T_2}+\frac{1}{16}\right)\mathrm{d}T_1+\left(\frac{1}{8a}+\frac{7}{32}\beta_1 a\right)\mathrm{d}a. \tag{33}$$

Integrating Eq. (33) leads to

$$\int \mathrm{d}\left(\frac{b}{a}\right) = -\left(\frac{\mathrm{d}\phi}{\mathrm{d}T_2}+\frac{1}{16}\right)T_1 + \int\left(\frac{1}{8a}+\frac{7}{32}\beta_1 a\right)\mathrm{d}a. \tag{34}$$

The coefficient of T_1 in Eq. (34) must vanish. Therefore,

$$\phi = -\frac{1}{16}T_2+\phi_0 \tag{35}$$

where ϕ_0 is a constant. Thus, to an error of $O(\varepsilon^2)$, the expansion of u to second approximation in Eq. (15) is

$$\begin{aligned} u = a(\hat{t})\cos\left[\hat{t}\left(1-\frac{1}{16}\varepsilon^2\right)+\phi_0\right] &- \varepsilon\left[\frac{1}{4}\Lambda_1\sin 3\left[\hat{t}\left(1-\frac{1}{16}\varepsilon^2\right)+\phi_0\right]\right. \\ &+\frac{1}{12}\Lambda_2\sin 5\left[\hat{t}\left(1-\frac{1}{16}\varepsilon^2\right)+\phi_0\right] \\ &+\frac{1}{24}\Lambda_3\sin 7\left[\hat{t}\left(1-\frac{1}{16}\varepsilon^2\right)+\phi_0\right] \\ &\left.+\frac{1}{40}\Lambda_4\sin 9\left[\hat{t}\left(1-\frac{1}{16}\varepsilon^2\right)+\phi_0\right]\right] \end{aligned} \tag{36}$$

where Λ_i's are given in Appendix A.

Equation (36) represents the approximate analytical solution of Eq. (13). $a(\hat{t})$ is the asymptotic function for which the initial condition is $a(\hat{t})|_{\hat{t}=0} = a_0$. The constants ϕ_0 and a_0 can be calculated by applying the initial conditions of the system.

5 Numerical examples

The system characteristics such as mass, spring stiffness, viscosity, orifice diameter, etc. affect the values of the parameters ($\varepsilon, \beta_1, \beta_2, \beta_3, \beta_4$); and consequently the parameters ($\Lambda_1, \Lambda_2, \Lambda_3, \Lambda_4$) in approximate analytical solution via Eq. (36). Table 1 exhibits the selected values for the numerical examples in this paper.

For instance, with the selected values for the first case, i.e., ($k = 1000$ N m^{-1}, $m = 20$ kg, $\mu = 0.0490$ Pa s, $D = 20$ cm, $d = 4$ cm), the amount of

Table 1 The selected values and the affected parameters for the numerical examples for $n = 1$ and $s = \frac{1}{2}$

Case	Selected values*					Affected parameters**							
	m (kg)	k (N m^{-1})	μ (Pa s)	u_0 (m)	v_0 (m s^{-1})	c_{lin} (N s m^{-1})	ω (rad s^{-1})	λ	ε	β_1	β_2	β_3	β_4
1	20	1000	0.049	0	0.9	7.1	7.07	0.012	0.05	208.3	16059	5.42×10^5	6.78×10^6
2	20	1000	0.147	0	0.9	21.2	7.07	0.036	0.15	208.3	16059	5.42×10^5	6.78×10^6
3	20	1000	0.294	0	0.9	42.5	7.07	0.072	0.3	208.3	16059	5.42×10^5	6.78×10^6
4	20	1000	0.490	0	0.9	71	7.07	0.12	0.5	208.3	16059	5.42×10^5	6.78×10^6
5	15	3×10^6	2.34	0.1	15	73	447	0.59	0.01	208.3	16059	5.42×10^5	6.78×10^6

* For all cases, $d = 4$ cm, $D = 20$ cm and $L = 1$ cm

** The parameters β_i are affected by n, s and γ

the affected parameters are computed as ($c_{\text{Linear}} = 7.1\ \text{N m s}^{-1}$, $\omega = 7.07\ \text{rad s}^{-1}$, $\lambda = 0.012326$, $\varepsilon = 0.05$, $\beta_1 = 208.3$, $\beta_2 = 16059.0$, $\beta_3 = 5.425 \times 10^5$, $\beta_4 = 6.782 \times 10^6$). Substituting these parameters into Eq. (26b) and Eq. (36) and applying the initial values ($u_0 = 0$ and $\dot{u}_0 = 0.9\ \text{m s}^{-1}$ for this case), one can easily obtain

$$a(t) = \frac{5000}{\sqrt{-1.302 \times 10^9 + 2\text{e}^{0.355t+21.079}}} \tag{37}$$

and

$$\begin{aligned} u(t) = a\cos(7.0700t + \phi_0) - \big(&46551.6a^9 \\ &+ 4787.8a^7 + 188.9a^5 + 3.27a^3\big) \\ &\times \sin(21.210t + 3\phi_0) - \big(1108.3a^9 + 88.67a^7 \\ &+ 2.1a^5\big)\sin(35.350t + 5\phi_0) - \big(193.9a^9 \\ &+ 8.87a^7\big)\sin(49.490t + 7\phi_0) - \big(16.625a^9\big) \\ &\times \sin(63.630t + 9\phi_0). \end{aligned} \tag{38}$$

For this case, the analytical solution of the simple mass–spring–damper system with the linear damper, is evaluated using Eq. (10) as follows:

$$u(t) = 0.1273\text{e}^{-0.1775t}\sin(7.0688t). \tag{39}$$

6 Results and discussion

In order to verify the accuracy of the solution (36), the numerical integration using the fourth-order Runge–Kutta method is applied. Figure 3(a) shows the comparison between the approximate analytical solution (38) and the numerical results obtained by Runge–Kutta method for the case (1). It can be seen that the approximate analytical solution is nearly identical to the results obtained by Runge–Kutta method. This comparison is carried out for the other cases given in Table 1 as well as case (1); and is illustrated in Figs. 3(b), 3(c), and 3(d). According to Fig. 3, as the value of ε rises, the error between the approximate analytical and the exact numerical solutions of Eq. (13) grows. This is due to the properties of the multiple scales method, whereas the value of ε must be small. Thus, the approximate analytical solutions are satisfactory for each case. In addition, Fig. 3 exhibits the responses of the system with the NDD damper and the system with the traditional linear damper, for different values of ε. The amplitude of the system with the NDD damper compared to the system with the linear damper is reduced in all cycles. The amount of vibration amplitude reduction for the case 1 with $\varepsilon = 0.05$, is 4.5 % in the first cycle, 16.2 % in the second cycle, 21.5 % in the third cycle, and 24.5 % in the fourth cycle. Table 2 shows the percentage of amplitude reduction in the other cases. It can be seen that for the higher values of ε, and hence the stronger nonlinearity; the percentage of the amplitude reduction in each cycle is more. Therefore, Table 2 clearly demonstrates the NDD damper performance in reducing the amplitude of the vibration system.

Figure 4 illustrates the damping force versus time for systems with the linear and the NDD damper. It clarifies the performance of the NDD damper from another point of view; and explains why the amplitude of the system with the NDD damper has been reduced. According to Eq. (11), damping force equals damping coefficient multiply by velocity. The damping coefficient of the linear damper is constant, so its damping force curve is sinusoidal. As mentioned earlier, the damping coefficient of the NDD damper is displacement-dependent, and as a result, the damping force curve of the NDD damper acts differently. It is observed that Fig. 4 can be divided into two zones; one with high and effective damping force and the other with low and ineffective damping force. The time that takes the curve of the NDD damper to pass through the effective zone is much longer than the

Table 2 The percentage of amplitude reduction in each cycle

Case	ε	Cycle					
		1	2	3	4	5	6
1	0.05	4.5	16.2	21.5	24.5	26.4	27.6
2	0.15	8.9	25.3	28.9	30.0	30.5	30.7
3	0.30	11.4	29.4	30.9	31.1	31.1	31.1
4	0.50	12.3	31.4	31.8	31.8	31.8	31.8

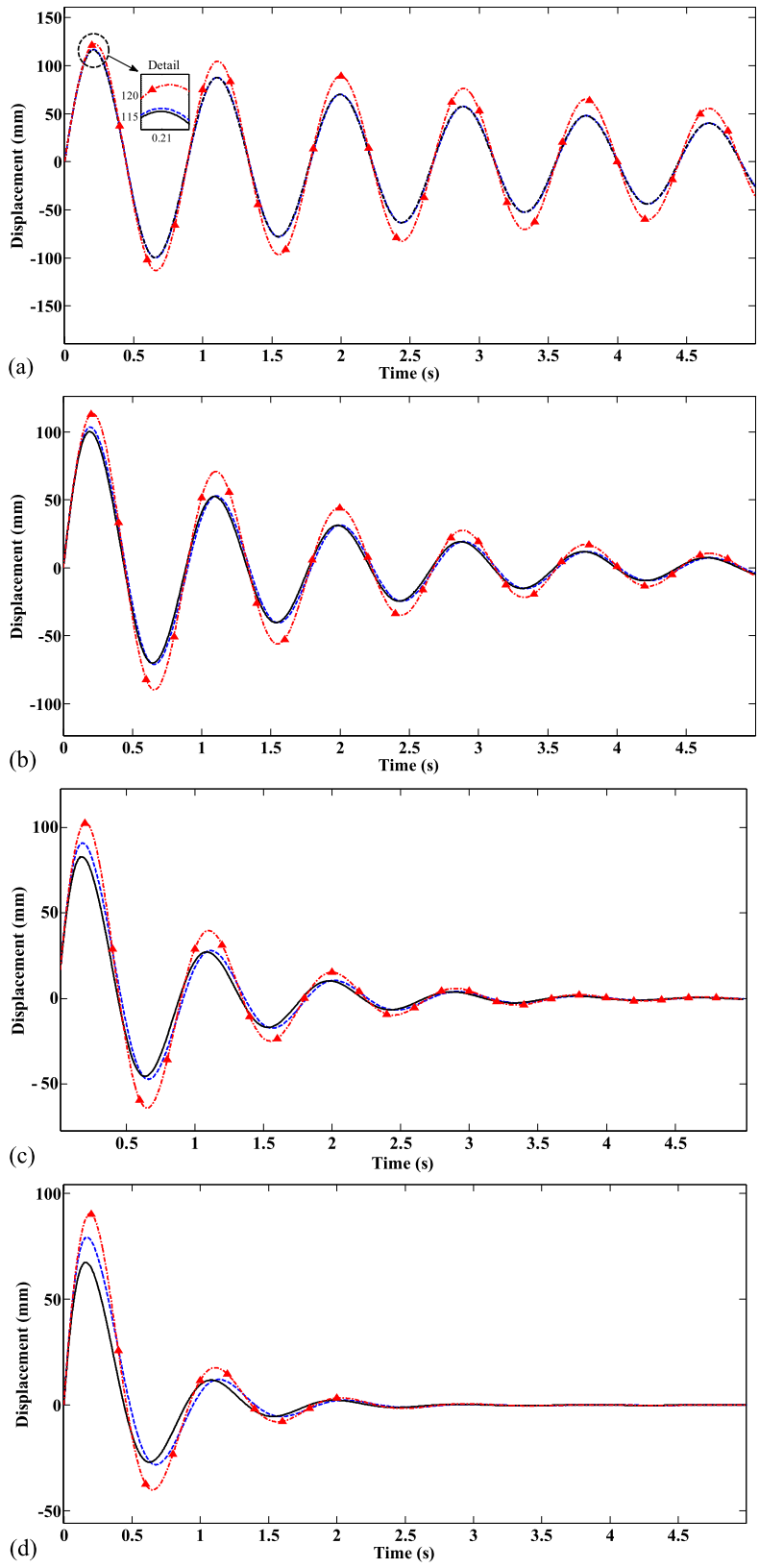

Fig. 3 Comparison between the approximate analytical solution and the numerical solution of Eq. (13) and the analytical solution of the system with the linear damper for (**a**) $\varepsilon = 0.05$ (**b**) $\varepsilon = 0.15$ (**c**) $\varepsilon = 0.30$ (**d**) $\varepsilon = 0.50$: ——— approximate analytical solution of the system with the NDD damper; – – – numerical solution of the system with the NDD damper; —·▲·— analytical solution of the system with the linear damper

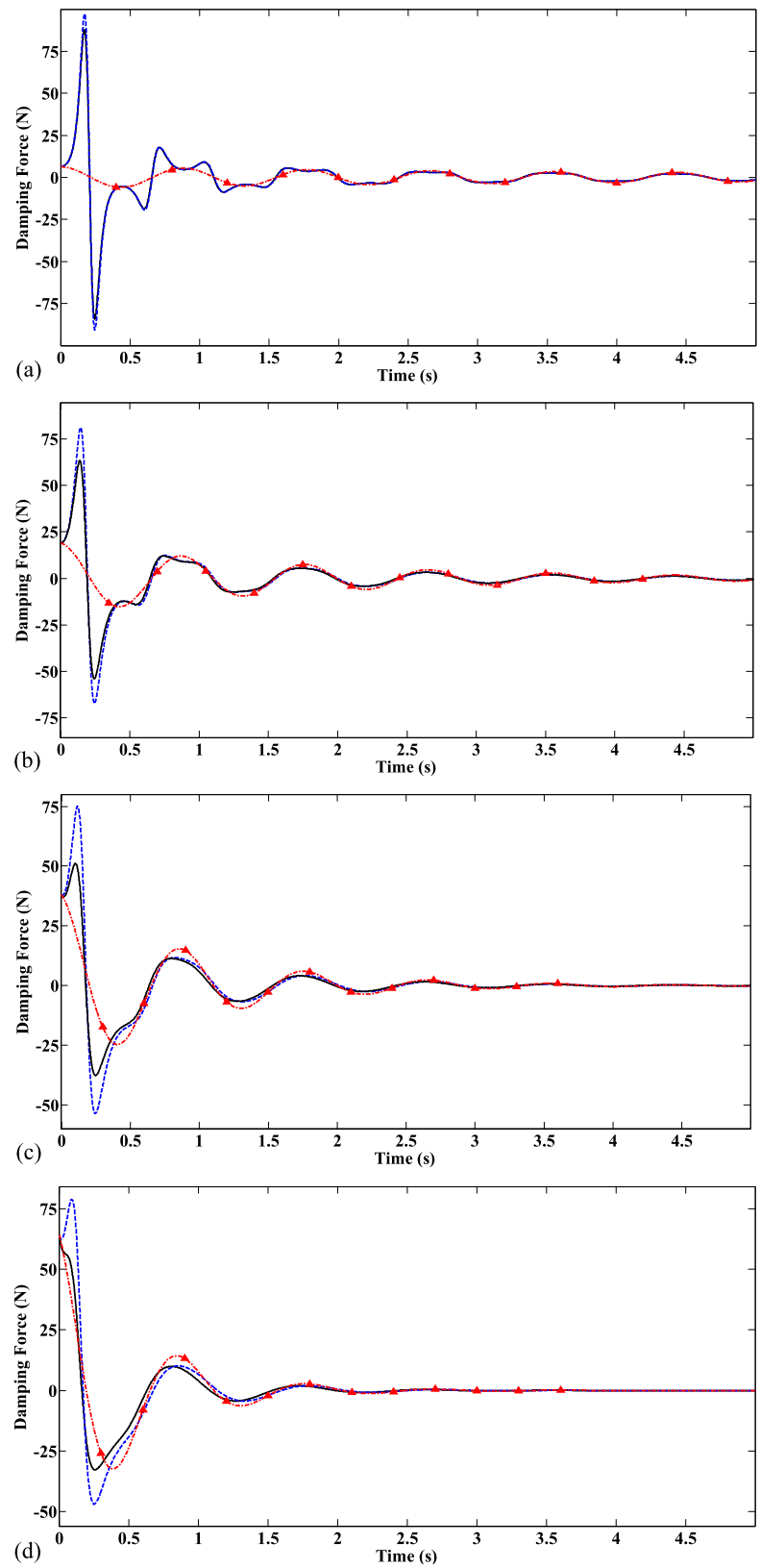

Fig. 4 Comparison between the damping force of the NDD damper obtained by multiple scales and Runge–Kutta methods and the damping force of the linear damper for (**a**) $\varepsilon = 0.05$ (**b**) $\varepsilon = 0.15$ (**c**) $\varepsilon = 0.30$ (**d**) $\varepsilon = 0.50$: ——— damping force of the NDD damper obtained by MSM; – – – damping force of the NDD damper obtained by the Runge–Kutta method; —·—▲—·— damping force of the linear damper

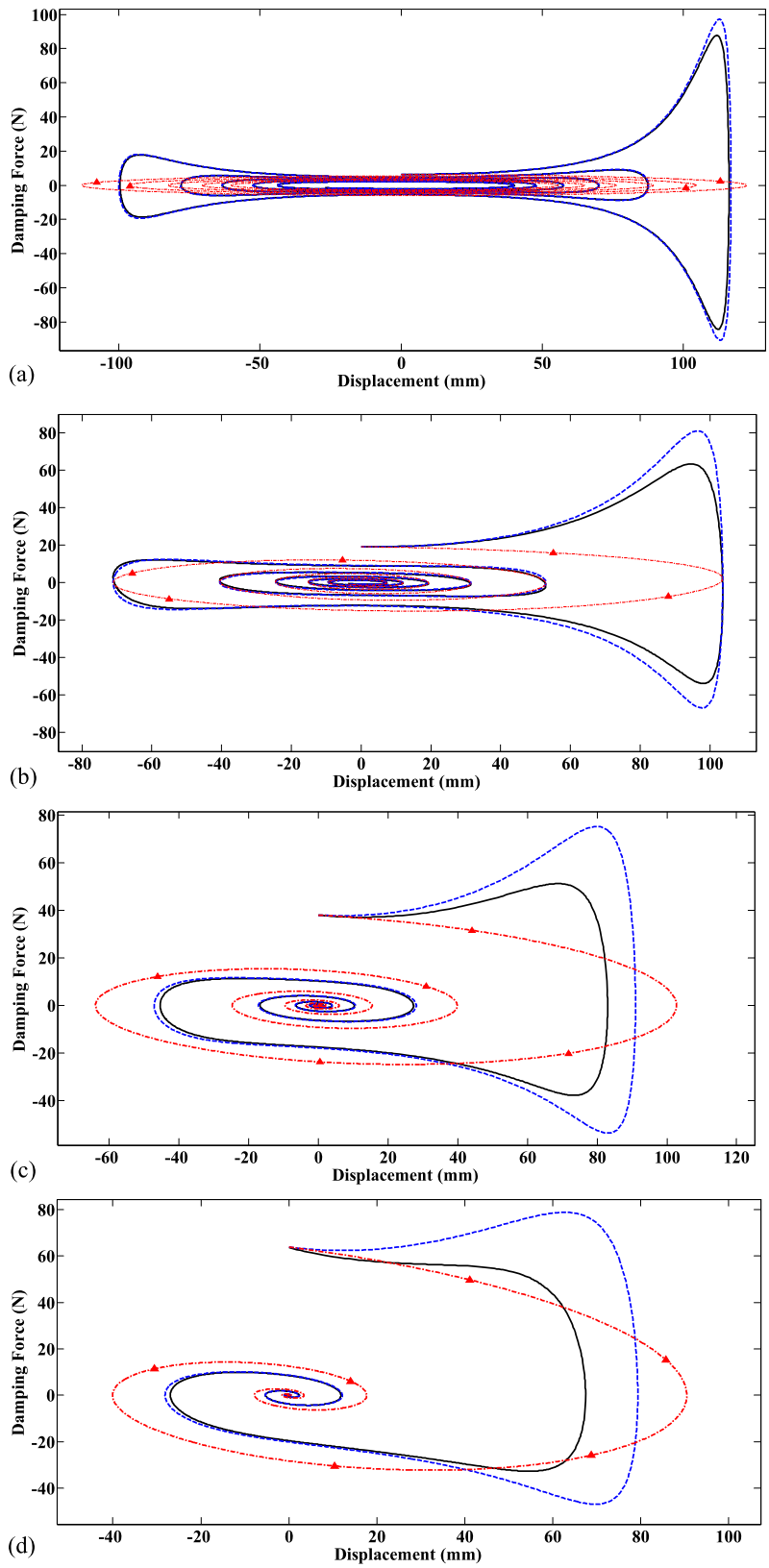

Fig. 5 Comparison between the damping force of the NDD damper versus displacement obtained by the multiple scales and the Runge–Kutta method and the damping force of the linear damper versus displacement for (**a**) $\varepsilon = 0.05$ (**b**) $\varepsilon = 0.15$ (**c**) $\varepsilon = 0.30$ (**d**) $\varepsilon = 0.50$: ——— damping force of the NDD damper obtained by MSM; – – – damping force of the NDD damper obtained by Runge-Kutta method; —·▲·— damping force of the linear damper

curve corresponding to the linear damper, because the curve of the NDD damper attains a maximum and then descends, while the other is decreasing and leaves this zone quickly. On the contrary, the curve of the NDD damper has a steep slope in the ineffective zone, while the curve slope of the linear damper is relatively gentle in this zone. This means that the curve of the linear damper stays in the ineffective zone for a longer time than the curve corresponding to the NDD damper. Moreover, according to the curve of damping force versus displacement shown in Fig. 5, and due to the fact that the area under force-displacement curve represents the work done, the NDD damper provides more energy dissipation capacity than the linear damper.

These all implies that for the aforementioned cases the NDD damper produces more effective force of opposite direction than the linear damper, so more energy dissipation occurs, particularly in the first cycle during the use of the NDD damper.

In addition, it is worthwhile to note that after a long period of time, the damping force related to the NDD damper get closer to the damping force related to the linear damper, because of the reduction of the amplitude which causes the drastic weakening of nonlinear terms in Eq. (13), as depicted in Figs. 4 and 5.

The scheme can be challenged by raising a question about the necessity of application of the NDD damper, while a simple linear damper with a higher damping coefficient is capable of reducing the amplitude of the vibration system. This can be exemplified by increasing the damping coefficient of the linear damper in order to achieve the behavior similar to the case that the NDD damper is used with $\varepsilon = 0.15$, as demonstrated in Fig. 6. The amount of the increased damping coefficient is specified as 33 $\mathrm{N\,m\,s^{-1}}$. For this damping coefficient value, the force transmitted to the base versus time, before and after increasing the damping coefficient, is shown in Fig. 7. As can be seen in Fig. 7, compared to the system with the NDD damper, increasing the damping coefficient in the system with the linear damper causes a considerable increase in the initial transmitted force. By decreasing the initial transmitted force, the initial impact applied to the system equipped with the NDD damper is also diminished. This feature shows the main advantage of the NDD damper compared with the traditional linear damper.

Case (5) of Table 1 characterizes the NDD damper performance when used in a high-frequency system. In Fig. 8, the approximate analytical solution of this case is verified by forth-order Runge–Kutta method. Figure 9 shows the comparison between the displacement of the system with the NDD damper and the system with the linear damper. For this case, the amounts of vibration amplitude reductions are computed as 15.03 % in the 10th cycle, 19.50 % in the 20th cycle, 21.53 % in the 30th cycle, 23.15 % in the 50th cycle, 23.33 % in the 70th cycle, and 23.37 % in the 100th cycle. Therefore, the use of the NDD damper scheme in high-frequency systems is also advantageous compared with the traditional linear damper.

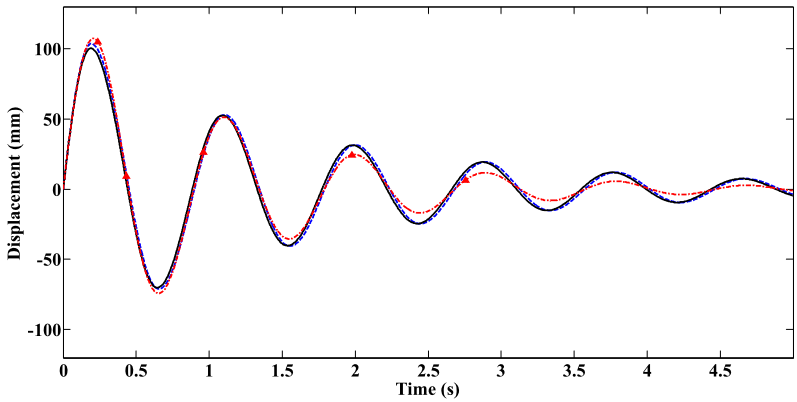

Fig. 6 Comparison of the amplitude of the system using the NDD damper with $\varepsilon = 0.15$ and the amplitude of the simple mass–spring–damper system with increased damping coefficient: ——— approximate analytical solution of the system with the NDD damper; - - - numerical solution of the system with the NDD damper; —·▲·— analytical solution of the system with increased linear damping coefficient

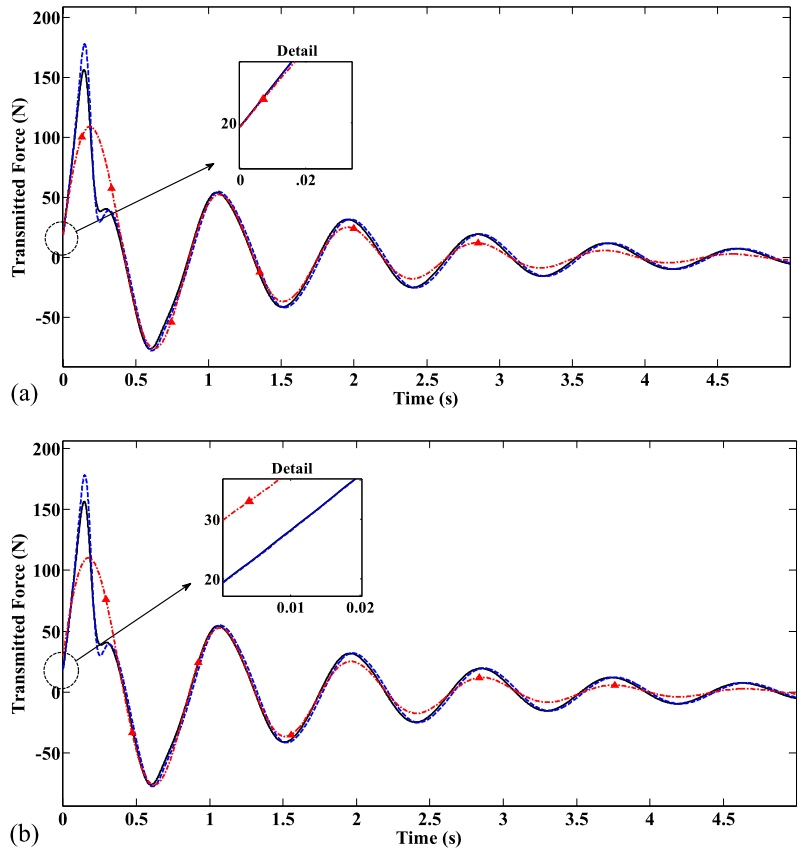

Fig. 7 Comparison of the transmitted force of the system using the NDD damper with $\varepsilon = 0.15$ obtained by the multiple scales and Runge–Kutta methods with the damping force of the linear damper (**a**) before increasing the linear damper coefficient (**b**) after increasing the linear damper coefficient: damping force of the NDD damper obtained by MSM; damping force of the NDD damper obtained by the Runge–Kutta method; damping force of the linear damper

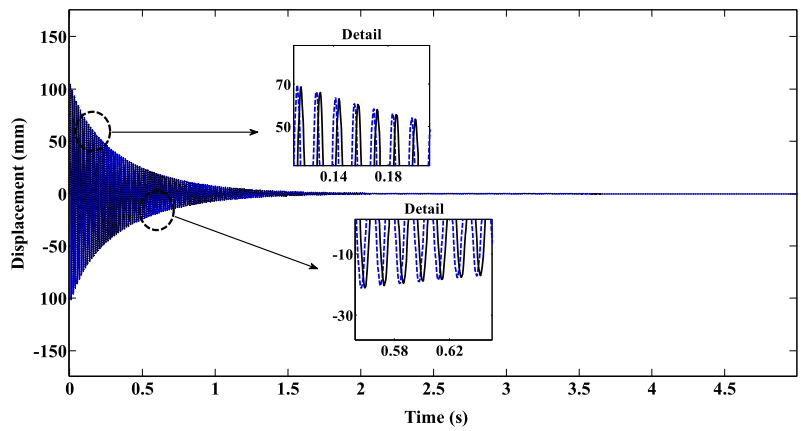

Fig. 8 Comparison between the approximate analytical and the exact numerical solutions of case (5) with $\varepsilon = 0.01$ for the system with the NDD damper: approximate analytical solution; exact numerical solution

As mentioned before, the area under force-displacement curve of a damper represents the amount of the dissipated energy. Figure 10 illustrates the comparison between the force-displacement curve of the NDD and the linear dampers. According to this figure in each cycle, the area under force-displacement curve of the NDD damper is larger than the corresponding area of the linear damper. Thus, the more reduced amplitude of the high-frequency system equipped with the NDD damper is caused by the more energy dissipated by this damper.

7 Conclusions

The performance of a nonlinear displacement-dependent (NDD) damper was studied. The NDD damper

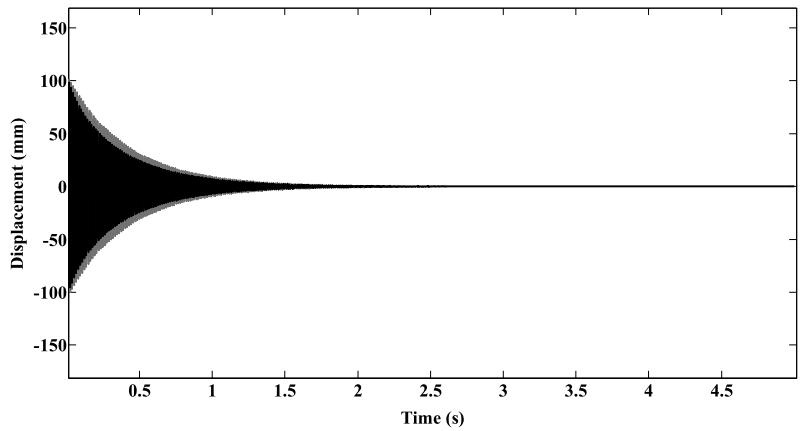

Fig. 9 Comparison between the approximate analytical solution of case (5) using the NDD damper with $\varepsilon = 0.01$, and the analytical solution of the system of case (5) with the linear damper: ——— approximate analytical solution of the system with the NDD damper; ——— analytical solution of the system with the linear damper.

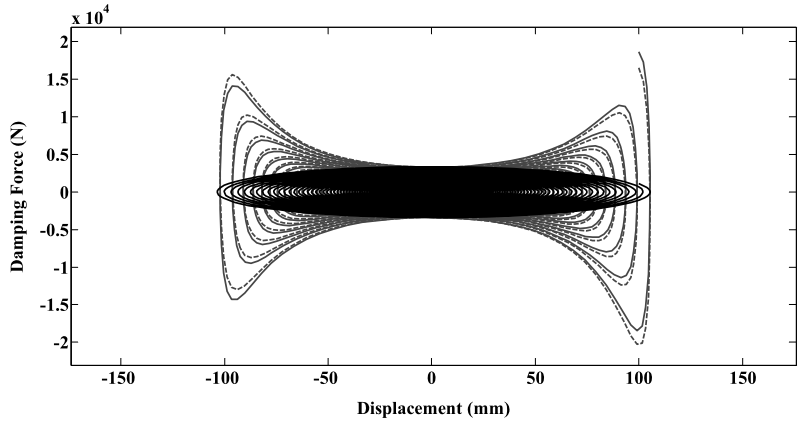

Fig. 10 Comparison of the force-displacement curve of the NDD damper obtained by multiple scales and the Runge–Kutta method for the case (5) with $\varepsilon = 0.01$ with the force-displacement curve of the linear damper: — — — damping force of the NDD damper obtained by MSM; ——— damping force of the NDD damper obtained by Runge–Kutta method; ——— damping force of the linear damper

mechanism was elaborated and the nonlinear governing differential equation describing a mass–spring–damper system equipped with the NDD damper was derived. Moreover, the free response of the system was obtained by the method of multiple scales as the approximate analytical approach, and then verified by numerical fourth-order Runge–Kutta method for several case studies. The simulation results demonstrated that the proposed NDD damper scheme along with the multiple scales method was not only able to achieve satisfactory response performance but also was feasible for vibration reduction in both low- and high-frequency systems. For the initial conditions under which the large amplitude is produced, the NDD damper was shown to have superior performance in reducing vibrations rather than the traditional linear damper. Furthermore, it should be mentioned that although increasing the damping coefficient in the system equipped with the traditional linear damper can reduce the amplitude of vibration as well as using the NDD damper, the initial transmitted force is considerably increased.

Appendix A

$$\begin{aligned}
\alpha_1 &= \left(\gamma^4 - 2\gamma^2 + 1\right)\lambda,\\
\alpha_2 &= \left(4\gamma^4 - 4\gamma^2\right)\lambda\beta,\\
\alpha_3 &= \left(6\gamma^4 - 2\gamma^2\right)\lambda\beta^2,\\
\alpha_4 &= \left(4\gamma^4\right)\lambda\beta^3,\\
\alpha_5 &= \left(\gamma^4\right)\lambda\beta^4,
\end{aligned} \tag{40}$$

$$\begin{aligned}
\Delta_2 &= \beta_2 A^3 + 3\beta_3 A^4 \bar{A} + 9\beta_4 A^5 \bar{A}^2\\
&\quad + 28\beta_5 A^6 \bar{A}^3,\\
\Delta_3 &= \beta_3 A^5 + 5\beta_4 A^6 \bar{A} + 20\beta_5 A^7 \bar{A}^2,\\
\Delta_4 &= \beta_4 A^7 + 7\beta_5 A^8 \bar{A},\\
\Delta_5 &= \beta_5 A^9,
\end{aligned} \tag{41}$$

$$
\begin{aligned}
q(T_1, T_2) = {} & \frac{1}{8}\beta_1^2 A^3 \bar{A}^2 + \beta_1\beta_2 A^4 \bar{A}^3 \\
& + \frac{23}{12}\beta_2^2 A^5 \bar{A}^4 + \frac{15}{4}\beta_1\beta_3 A^5 \bar{A}^4 \\
& + 14\beta_2\beta_3 A^6 \bar{A}^5 + 14\beta_1\beta_4 A^6 \bar{A}^5 \\
& + \frac{1205}{48}\beta_3^2 A^7 \bar{A}^6 + \frac{154}{3}\beta_2\beta_4 A^7 \bar{A}^6 \\
& + \frac{13013}{40}\beta_4^2 A^9 \bar{A}^8, \qquad (42)
\end{aligned}
$$

$$
\begin{aligned}
\Lambda_1 &= 3.708 \times 10^5 a^9 + 3.8146 \times 10^4 a^7 \\
&\quad + 1.505 \times 10^3 a^5 + 26.041 a^3, \\
\Lambda_2 &= 2.65 \times 10^5 a^9 + 2.1193 \times 10^4 a^7 \\
&\quad + 5.018 \times 10^2 a^5, \qquad (43) \\
\Lambda_3 &= 9.2718 \times 10^4 a^9 + 4.2385 \times 10^3 a^7, \\
\Lambda_4 &= 1.3245 \times 10^4 a^9.
\end{aligned}
$$

References

1. Dixon, J.C.: The Shock Absorber Handbook, 2nd edn. Wiley, Chichester (2007)
2. Eslaminasab, N.: Development of a semi-active intelligent suspension system for heavy vehicles. Ph.D. Thesis, University of Waterloo, Canada (2008)
3. Zhou, N., Liu, K.: A tunable high-static–low-dynamic stiffness vibration isolator. J. Sound Vib. **329**, 1254–1273 (2010)
4. Cetin, S., Zergeroglu, E., Sivrioglu, S., Yuksek, I.: A new semiactive nonlinear adaptive controller for structures using MR damper: design and experimental validation. Nonlinear Dyn. **66**(4), 731–743 (2011)
5. Dong, X.-M., Yu, M., Liao, C.-R., Chen, W.-M.: Comparative research on semi-active control strategies for magneto-rheological suspension. Nonlinear Dyn. **59**, 433–453 (2010)
6. Song, X., Ahmadian, M.: Characterization of semi-active control system dynamics with magneto-rheological suspensions. J. Vib. Control **16**(10), 1439–1463 (2010)
7. Go, C.-G., Sui, H., Shih, M.-H., Sung, W.-P.: A linearization model for the displacement dependent semi-active hydraulic damper. J. Vib. Control **16**(14), 2195–2214 (2010)
8. Simon, D.E.: Experimental evaluation of semiactive magneto-rheological primary suspensions for heavy truck applications. Ph.D. Thesis, Virginia Tech (2000)
9. Preumont, A.: Vibration Control of Active Structures. Kluwer Academic, Dordrecht (2002). EBook ISBN: 0-306-48422-6
10. Crosby, M.J., Karnopp, D.C.: The active damper. Shock Vib. Bull. **43** (1973)
11. Ahmadian, M.: On the isolation properties of semiactive dampers. J. Vib. Control **5**(2), 217–232 (1999)
12. Alanoly, J., Sankar, S.: A new concept in semi-active vibration isolation. In: ASME Design Engineering Technical Conference, t86-DET-28 (1986)
13. Venkatesan, C., Krishnan, R.: Harmonic response of a shock mount employing dual-phase damping. J. Sound Vib. **40**(3), 409–413 (1975)
14. Haque, M.M., Ahmed, A.K.W., Sankar, S.: Simulation of displacement sensitive non-linear dampers via integral formulation of damping force characterization. J. Sound Vib. **187**, 95–109 (1995)
15. Hundal, M.S.: Impact absorber with two-stage variable area orifice hydraulic damper. J. Sound Vib. **50**(2), 195–202 (1977)
16. Fukushima, N., Hidaka, K., Iwata, K.: Optimum characteristics of automotive shock absorbers under various driving conditions and road surfaces. In: JSAE Review, pp. 62–69 (1983)
17. Jackson, G.W.: Fundamentals of the direct acting shock absorber. SAE paper 37R, National Passenger Car Body and Materials Meeting, Detroit (1959)
18. Puydak, R.C., Auda, R.S.: Designing to achieve optimum dynamic properties in elastomeric cab and body mounts. SAE 660439 (and SAE Transactions V75) (1966)
19. Lewitske, C., Lee, P.: Application of elastomeric components for noise and vibration isolation in the automotive industry. SAE Paper 2001-01-1447 (2001)
20. Lee, C.-T., Moon, B.-Y.: Study on the damping performance characteristics analysis of shock absorber of vehicle by considering fluid force. J. Mech. Sci. Technol. **19**(2), 520–528 (2005)
21. Lee, C.-T., Moon, B.-Y.: Simulation and experimental validation of vehicle dynamic characteristics for displacement-sensitive shock absorber using fluid-flow modeling. Mech. Syst. Signal Process. **20**, 373–388 (2006)
22. Young, D.W.: Aircraft landing gears. Proc. Inst. Mech. Eng. **200**(D2), 75–92 (1986)
23. Komamura, S., Mizumukai, K.: History of shock absorbers. Automob. Technol. **41**(1), 126–131 (1987) (in Chinese)
24. Farjoud, A., Ahmadian, M., Craft, M., Burke, W.: Nonlinear modeling and experimental characterization of hydraulic dampers: effects of shim stack and orifice parameters on damper performance. Nonlinear Dyn. **67**(2), 1437–1456 (2012)
25. Guo, P.F., Lang, Z.Q., Peng, Z.K.: Analysis and design of the force and displacement transmissibility of nonlinear viscous damper based vibration isolation systems. Nonlinear Dyn. **67**(4), 2671–2687 (2012)
26. Rao, S.S.: Mechanical Vibrations, 4th edn. Prentice-Hall, Englewood Cliffs (2004)
27. Nayfeh, A.H., Mook, D.T.: Nonlinear Oscillations. Wiley, New York (1979)
28. Nayfeh, A.H.: Perturbation Methods. Wiley, New York (1973)